Operation of a low power Hall thruster with a shielded magnetically configuration

IEPC-2019-619

Presented at the 36th International Electric Propulsion Conference
University of Vienna • Vienna, Austria
September 15-20, 2019

L. Garrigues[1], S. Santhosh[2]
LAPLACE, Université de Toulouse, CNRS, 118 route de Narbonne, 31062 Toulouse, Cedex 9, France

L. Grimaud[3] and S. Mazouffre[4]
ICARE, CNRS, 1C avenue de la recherche scientifique, 45071 Orléans Cedex, France

Abstract: Two different magnetic field topologies have been modeled using an hybrid PIC/fluid approach in the context of a low poser Hall thruster. The first topology corresponds to a standard (unshielded) magnetic field configuration where the maximum of magnetic field strength is located in the exhaust plane. The second topology characterized by a maximum of strength in the near field plume and almost parallel-to-walls direction of magnetic field inside the channel. This second topology is referred to magnetic shielded configuration in the literature. In the magnetic shielding configuration, the shift of ionization and acceleration regions towards the near field plume accordingly contributes to the reduction of erosion. Moreover, inside the channel, the erosion is reduced since the cooling of the electron temperature diminishes the sheath potential drop and consequently the kinetic energy of ions impacting on channel walls. A larger fraction of doubly charged ions is also found in the shielded magnetic configuration.

I. Introduction

THE demand for low power Hall thrusters on small satellites (~ 100 kgs, ~ 200 W) operating in low-earth-orbit for commercial and scientific missions is continuously increasing. Standard Hall thrusters in the 200W-power range limit the mission duration of operation due to limited lifetime of thrusters (less than 2000 hours, [1]). In standard Hall thruster, the magnetic field lines are designed to focus the ions in the axial direction with the idea of equipotential electric potential lines following the magnetic field lines. The position of the maximum magnetic field is set to be in the exhaust region to trap electrons and generate ions at that location [2]. These basic ideas have to be revised for two reasons: 1) ions are generated deeper in the channel, 2) high electron temperature in exhaust region leads to a radial component of electric field larger than axial one close to the walls. The electric potential shape does not permit to ions generated out of channel axis to be focused in axial direction (see figure 1, left panels). Due large sheath potential drop associated to high electron temperature, ions bombard the walls with energies larger than erosion threshold, limiting the thruster lifespan.

---

[1] Director of Research at CNRS, LAPLACE, laurent.garrigues@laplace.univ-tlse.fr.
[2] PhD candidate, LAUM, sobin.santhosh@univ-lemans.fr
[3] Dr Engineer in electric propulsion, ENPULSION, lou.grimaud@enpulsion.com.
[4] Director of Research at CNRS, ICARE, stephane.mazouffre@cnrs-orleans.fr

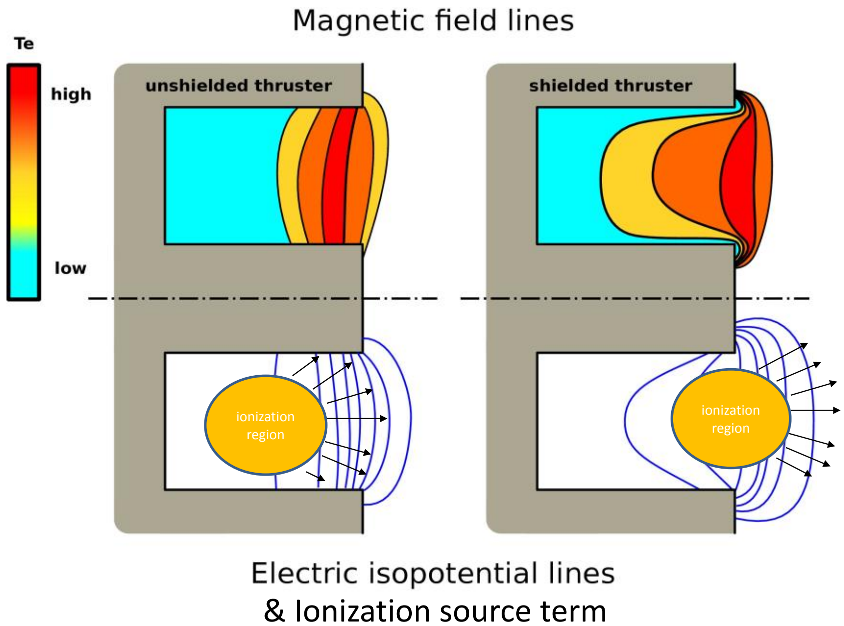

Figure 1. Comparison between standard and magnetically shielded Hall thruster configurations.

The magnetic field topology has been modified to prevent or limit ion bombardment on channel walls. The main characteristic of the so-called magnetic shielding configuration is the presence of field line tangent to the wall reaching from the thruster's magnetic poles to the anode area. This "grazing line" produces a layer of low energetic electrons near to the walls and thus reduces the sheath potential drop. In order to get this grazing line the maximum of the magnetic field needs to be pushed downstream of the exit plane of the thruster. In a shielded configuration, the ionization and acceleration regions are mostly situated outside the thruster (see figure 1, right panels). Consequently, the electron temperature inside the channel is low and electric potential lines now almost follow the magnetic field lines as illustrated figure 1. Helped by a conical shape of the downstream channel aperture, the new magnetic configuration offers a reduction of wall erosion by a decrease of both ion flux and energies [3-8]. The goal of this paper is to revisit the common issues of magnetically shielded effect in the context of the study of the ISCT-200 low power Hall thruster built and tested at the ICARE laboratory in Orléans, France [6-8].

In the rest of the paper, we briefly described the hybrid PIC/fluid model in section II. Computational results are detailed in section III. Section IV summarizes and gives perspectives to that work.

II. Overview of the hybrid PIC/fluid model

The hybrid PIC/fluid model is two-dimensional (axial and radial directions are considered, namely x and r, respectively), axisymmetric, starting from the anode plane at the rear of the channel and ending at the magnetic field line that intercepts the cathode. The channel end is conical. The magnetic field is preprocessed and not modified by the self-magnetic field induced by the azimuthal Hall current. A kinetic description is used to calculate the transport of heavy species, while the electron transport is represented with fluid equations, assuming a Maxwellian distribution function. The model is quasineutral and sheaths are described analytically. The electron density is everywhere equal to ion density (referred to as plasma density in the rest of paper). Typically, 100 x 75 computational cells are used with a regular grid is inside the channel region and a sparse grid employed in the near field region.

A. Kinetic description of heavy species

The energy distribution of heavy species is sampled with a fixed number of macroparticles (also called superparticles in the literature). At each time step heavy species trajectories are integrated according to Newton's law, ions remaining unmagnetized. In the discharge volume, new ions are generated according to the spatial profile of ionization source term, and neutral atoms are depleted accordingly. Ion species taken into account are singly (xenon ground state to first level of ionization of charge) and doubly charged ions (from ground state to second level of ionization and the stepwise ionization from first level of ionization to second level of ionization). The rates are the same as in the study of Ref. [9]. Ions impinging the walls of the channel and the anode plane are neutralized and new neutrals return back in the computational domain, while ions passing the cathode line are eliminated. Neutrals are injected in the simulation domain through the injection region according to the mass flow. Neutrals colliding with walls are isotropically reflected according to a half Maxwellian distribution in the direction normal to the surface at a temperature of T_w = 500 K [10]. Neutrals crossing the open Cartesian boundary beyond the cathode line are eliminated. A supplementary injection of neutrals to account for the vacuum backpressure is also included.

A specific attention has been put in the fulfillment of the Bohm criterion of ions at the sheath entrance using a forcing method [10], [11]. We define a strip d_w at a small distance of the walls (typically d_w ~ 150 μm, larger than $c_s\Delta t$ – c_s being the sound speed, i.e. typically half the cell thickness adjacent to the wall) in which we calculate the Bohm velocity for singly and doubly charged ions. For the particles located in those strip, we add an increment of velocity in the component normal to the wall such that the ion mean velocity equals the Bohm velocity.

The estimation of thruster wall erosion has been considered including in the model a calculation of sputtering processes under ion bombardment on the walls, the effect of neutrals is negligible since their energy is much smaller compared to that of ions (no fast neutrals are considered). The effect of re-deposition is neglected too. To determine the axial profile of erosion, we have calculated the eroded thickness per unit time that depends on the ion flux at the walls, the properties of the wall and the sputtering yield Y (number of atoms ejected per incident ions). We use the same method as in Ref. [15] with a sputtering energy threshold fixed to 30 eV.

B. Fluid electron transport

We use a fluid collisional approach (three firsts moments of Boltzmann equation) to describe the electron transport, coupled with a quasineutral assumption. The plasma density n is obtained from the calculations of ion densities with the PIC sub-model:

$$n = n_{i^+} + 2n_{i^{2+}} \quad (1),$$

where n_{i^+} and $n_{i^{2+}}$ are respectively singly and doubly charged ion densities. The electric potential profile is no longer calculated from the Poisson's equation but from the coupling of electron momentum and continuity equations.

It is convenient to treat the electron transport in the two directions separately to construct a grid aligned on the magnetic field lines. The magnetic streamlines λ are obtained from:

$$\frac{\partial\lambda}{\partial x} = rB_r, \frac{\partial\lambda}{\partial r} = -rB_x \quad (2),$$

B_r and B_x being the radial and axial coordinates of magnetic field. The λ stream function is constant along the magnetic field lines ($\mathbf{B}.\nabla\lambda = 0$). The constructions of the stream function requiring a monotonic variation of λ, we have defined 4 zones connected by the X-point where fluid equations are solved independently.

Along the magnetic field lines, an electron momentum equation under the drift-diffusion approximation in which the drift and diffusion terms are almost the same implies that the electric potential distribution can be determined from a Boltzmann's distribution. The electric potential is written under the form [13]:

$$\emptyset(x,r) = \emptyset^*(\lambda) + \frac{2}{3e}\varepsilon_e(\lambda)\ln\left[\frac{n(x,r)}{n_0}\right] \quad (3),$$

where the electron mean energy is denoted as ε_e, n_0 is a reference density (constant). $\emptyset^*$ called the thermalized potential and ε_e are functions depending on the λ stream function. For Maxwellian electrons, $\varepsilon_e = \frac{3}{2}T_e$.
The electric potential profile is the result of the imposed potential drop between anode and cathode and electron conductivity perpendicular to the magnetic field (generalized Ohm's law). Across the magnetic field lines, the electron flux is $\Gamma_{e,\perp}$ written as:

$$\Gamma_{e,\perp} = -\mu_{e,\perp}\left[nE_\perp + \frac{2}{3e}\nabla_\perp(n\varepsilon_e)\right] \quad (4),$$

where the index ⊥ indicates the direction perpendicular to the magnetic field, $\mu_{e,\perp}$ and $E_{\perp}$ respectively are the cross field electron mobility and electric field, and $\nabla_{\perp}$ is the cross field gradient. To calculate the electric field profile, we substitute in Eq. (4) the current conservation equation:

$$e\iint \Gamma_{e,\perp}ds = e\iint \Gamma_{i,\perp}ds - \beta I_d \quad (5),$$

$\Gamma_{i,\perp}$ is the cross field ion flux, e is the elementary charge, and integrals are taken along the magnetic field lines (surfaces). The discharge current I_d is determined such that a given potential drop is applied between anode and cathode, and β is equal to 0 (perfect dielectric) in zones where magnetic field lines connect the same wall.

We solve a one-dimensional energy equation perpendicular to magnetic field (integrated between two consecutive λ lines) to determine the electron mean energy profile that involves in the calculations of electric potential and ionization source terms. The energy equation is written as:

$$\frac{\partial(n\varepsilon_e)}{\partial t} + \frac{5}{3}\nabla_{\perp}.\left(\Gamma_{e,\perp}\varepsilon_e\right) - \frac{10}{9e}\nabla_{\perp}.\left(\mu_{e,\perp}n\varepsilon_e\nabla_{\perp}\varepsilon_e\right) = -eE_{\perp}.\Gamma_{e,\perp} - P^{col} - P^{W} \quad (6).$$

P^{col} and P^{W} corresponding to the energy losses due to inelastic collisions between electrons and heavy species and to electron-wall interactions inside the channel, are detailed in Refs. [9] and [15], respectively. More information about numerical techniques about the electron model is detailed in Refs. [14], [15].

One critical point of fluid transport of electrons is linked to the so-called "anomalous transport". We fit the anomalous collision profile ν_{an} to match time-averaged measured and calculated ion velocity profiles as in Ref. [16] (time averaged over a few hundreds of microseconds, larger than the time for the breathing mode). The magnitude of the frequency is chosen to match the discharge current. We show in Figure 2 a comparison between measured and calculated ion velocity profiles and frequency profiles along the thruster centerline for a mass flow of 1 mg.s^{-1} and a voltage of 300 V for the ICST200-US (unshielded) and ICST200-MS (shielded).

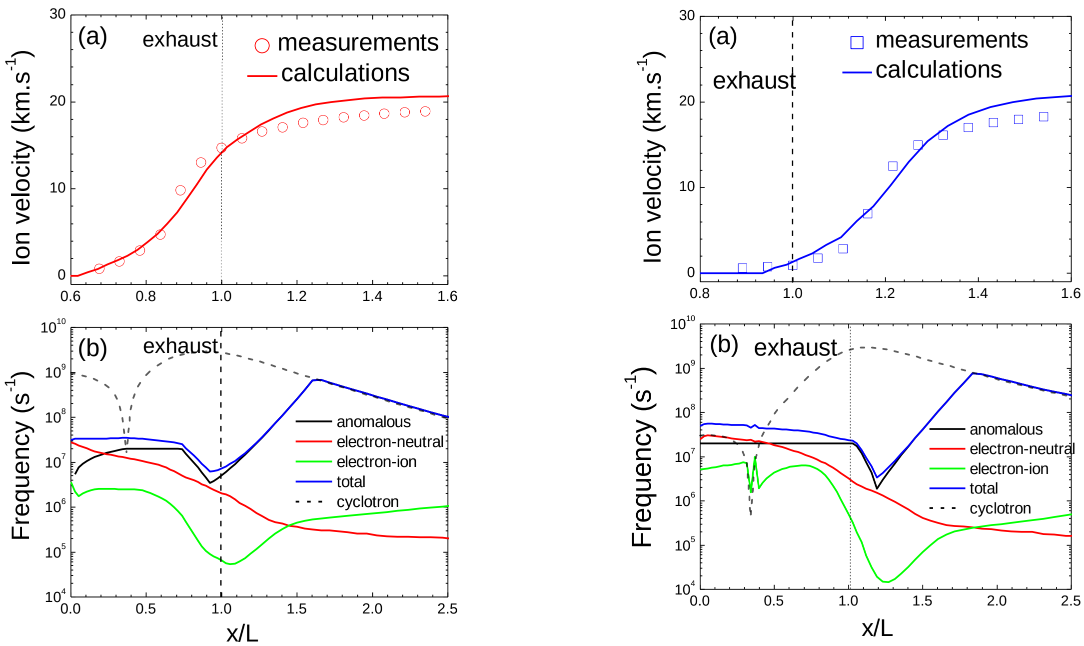

Figure 2. Profiles of ion velocity and collision frequencies along the thruster centerline. The xenon mass flow is 1 mg.s^{-1} and the voltage 300 V. Left panel US (unshielded) configuration and right panel MS (magnetically shielded) configuration.

The electron-neutral and electron-ion collision frequencies exhibit very similar profiles in the US and MS configurations, especially the contribution of electron-neutral collisions on the cross-field transport is important close to the anode where the gas is injected, while the electron-ion collisions play a negligible role on the cross-field transport. The anomalous collision frequency adjusted to match ion velocity profiles has an axial shift corresponding to the location of the maximum of magnetic field and drop of electron cross-field mobility. We have limited the anomalous frequency to the cyclotron frequency in the near field region. This rather arbitrary condition maintains that the electrons are magnetized in the near field plume, that it is consistent with the hypothesis of the model (in that situation, the Hall parameter H is equal to 1).

III. Comparisons between unshielded and shielded magnetically configuration

All the simulations have been performed for a fixed xenon mass flow rate of 1 mg/s and a discharge voltage of 300 V. The backpressure is fixed to 0.5 mPa. We only present time-averaged results over 1 ms of plasma properties and estimation of erosion rate in that paper.

A. Plasma properties

Time-averaged plasma properties of the US and MS configurations are depicted in figure 3. The axial and radial distances have been normalized to thruster channel length L and outer radius R. A comparison of electric potential profiles of Fig. 3a and 3d clearly exhibits a shift of the acceleration region, associated with a shift of the maximum of magnetic field. In this US configuration, the acceleration region takes place from either side of the exhaust plane, while the acceleration region is concentrated in the near field plume in the MS configuration. In the MS case, a closer look to the axial variation of the electric potential inside the channel near the inner and outer walls shows a nearly flat potential profile between 302 V ± 2.5 V, as previously shown in the literature [17]. In the MS configuration, a quasi-constant electric potential value (close to the discharge voltage) is obtained near the walls, while a drop of electric potential in the zone of strong magnetic field is observed in the US configuration [4]. In Figs 3a and 3d, the electric potential profile has a non-monotonic variation with a maximum on the channel centerline, close to the anode in the US configuration and close to the exhaust in the MS configuration. 2D Calculations of the MaSMi-60 operation reveal the same trend in the electric potential profile [17]. The maximum of potential drop is associated to the local electron temperature, few volts in the US configuration and 10 V in the MS configuration. Induced by gradient of plasma density, from that specific region, electrons reach the anode through diffusion (second term on the right-hand side of Eq. (4)). A qualitative comparison of electric potential lines and magnetic field lines agrees with scheme presented Figure 1. Inside the channel, the electric potential lens is concave in the US configuration and convex in the MS configuration.

Due to the shift of acceleration region, the electrons gain energy less deeply into the channel in the MS configuration, as shown in Figures 3b and 3e. The maximum of electron temperature is larger in the MS configuration 53 eV, to be compared with 30 eV in the US configuration. The maximum of Te is in the same range of 2D calculations of the MaSMi-60 [17] for a same voltage but a bit larger mass flow of xenon. In the MS configuration, a significant reduction of the electron temperature in the channel is visible (Te ≤ 10 eV), downstream the ionization region. The “grazing” line that connects the poles to the anode region leads to low energetic electrons coming from the anode region to be able to easily travel along the magnetic field lines, establishing a low electron temperature close to the walls. Near the inner and outer walls Te is almost constant (2 eV ± 1 eV). Experiments confirm that the electron temperature along the walls is between 2.5 and 3 times smaller in the MS configuration [4]. Unfortunately, same measurements have not been performed yet for low power MS Hall thrusters. One indirect confirmation of a lower electron temperature close to the walls in the MS configuration comes from the picture of the light emitted when both thrusters operate. While in the US configuration the light emission covers all the surface of the channel exhaust, a less intense zone exists close to the walls in the MS configuration [18]. This effect can be almost partially attributed to a lower electron temperature in the near-wall region in the MS case.

The ionization source terms including all the contributions to ionization processes are shown in Figures 3c and 3f. Axially, the ionization region starts from the region of zero-B field and stops at the end of the channel in the US and extends to the near-field plume in the MS configuration. The peak of ionization (almost the same for both configurations ~ 10^{24} $m^{-3}s^{-1}$) is spatially shifted in the exhaust plane in the MS case. One difference is the total ion current produced inside the discharge (calculated by integration of the local source term and volume time the charge number and elementary charge), it reaches 1.07 A in the US configuration and increases to 1.54 A in the MS configuration. Radially, the ionization region covers the entire channel region while a zone of very low ionization is visible near the walls in the MS configuration. The explanation is directly linked to the electron temperature profile. In the US configuration, a second zone of ionization appears, associated to the increase of magnetic field upstream the region of zero-B field. Keep in mind that no magnetic optimization has been performed for that version of the ICST-200.

The plot of ion flux vectors in Figs. 3c and 3e is very instructive. In both cases, we can easily delimitate a zone above which ions generated are directed towards the walls. This region depends on the ratio between radial and axial electric fields, since ions are not magnetized and created at almost zero energy. The magnitude of the ion current impacting on wall is linked to the local ionization source term. In the US case, the zone of ion losses corresponds to the anode region (where a maximum of electric potential exists – see fig.3a) and to the peripheral zone of ion generation, where ions are accelerated towards the walls due to the concave shape of electric potential. In the MS case, the main reason of ion losses is the presence of the peak of electric potential at 309 V in the exhaust region. As we see in Fig. 3e, ions are accelerated towards the walls when they are generated on the left-side of the ionization source term and towards the exhaust over wise. We will examine the thruster erosion in the next section. The positive effect of the conical shape of channel geometry on the reduction of ion impacts on walls is also visible in Fig. 3f, since the ion flux vectors are almost parallel to the walls. Nevertheless, we must point that this reduction is concentrated on a small area and underlines that it contributes to enlarge the divergence.

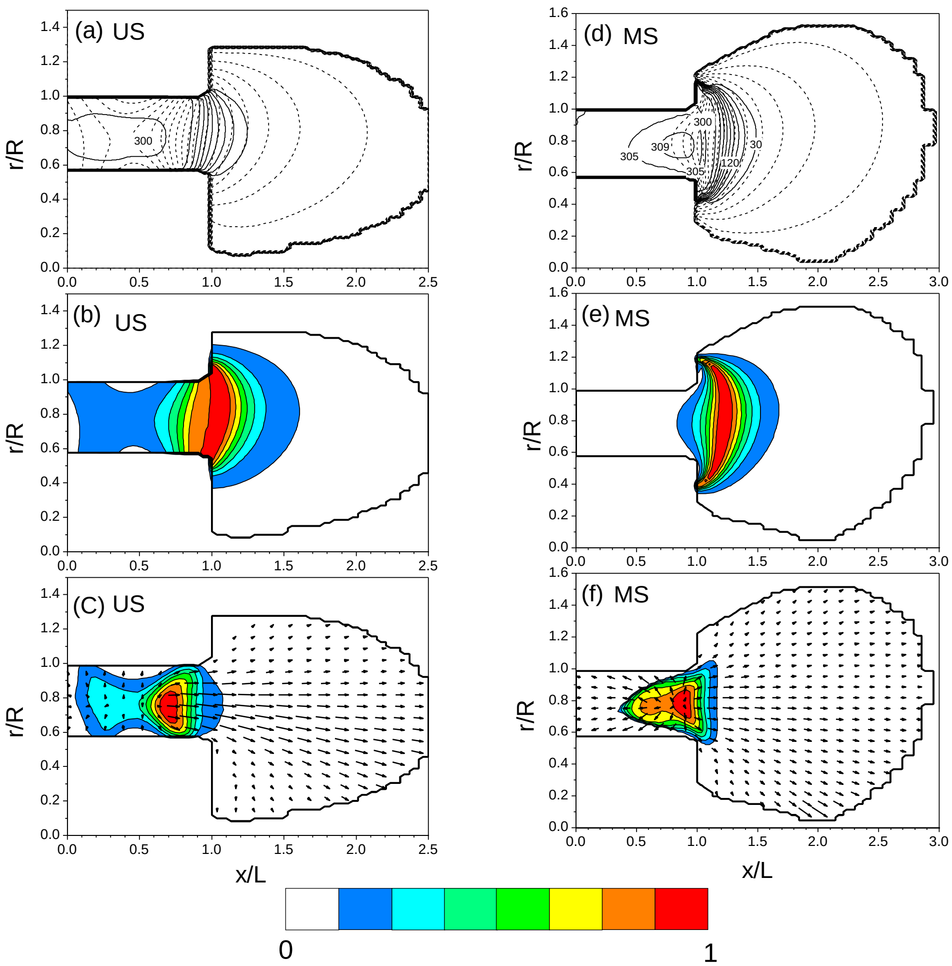

Figure 3. Time-averaged plasma properties (a) Contours of electric potential (from 0 to 300 V, 10 contours equally spaced) and magnetic field lines, (b) 2D profile of electron temperature (color scale, 8 contours equally spaced, maximum of 30 eV), (c) 2D profile of ionization source term (color scale, 8 contours equally spaced, maximum of 9.2×10^{23} m^{-3} s^{-1}) overlaid by ion flux vectors, (d) Contours of electric potential (from 0 to 300 V, 10 contours equally spaced, contours of 305 and 309 V are also shown) and magnetic field lines, (e) 2D profile of electron temperature (color scale, 8 contours equally spaced, maximum of 53 eV), (f) 2D profile of ionization source term (color scale, 8 contours equally spaced, maximum of 1.3×10^{24} m^{-3} s^{-1}) overlaid by ion flux vectors. Figures (a) to (c) correspond to the unshielded configuration (US), while figures (d) to (f) are related to the shielded configuration (MS). The xenon mass flow is 1 mg.s^{-1} and the voltage 300 V.

B. Erosion estimation

In figure 4, we compare the kinetic energy of the ions impacting on the walls and estimate the eroded thickness for 1000 hours of thruster operation for the two magnetic configurations. In Fig. 4a, in the US case, an increase of the mean kinetic energy of the ions impinging the walls is visible at x/L ≥ 0.6. The sheath potential drop in the region of strong electron temperature can reach 80 V. In the MS case, the sheath potential drop remains low and the mean energy stays almost independent of axial position and below 20 eV.

In figure 4b, the eroded thickness shown are only for a sputtering threshold of 30 eV (a larger value of threshold induces a thickness close to zero in the MS configuration). The positive effect of the conical shape of the walls close to the exhaust is visible with a reduction of the eroded thickness in the US case. In agreement with results of Figure 3, we notice a slight increase of eroded thickness downstream the zero-B position due to ions generated in that region and whose energy gained in the radial direction is higher than the sputtering threshold. Beyond a quantitative calculation of the wall erosion, the effectiveness of the MS configuration on the erosion of the walls is obvious.

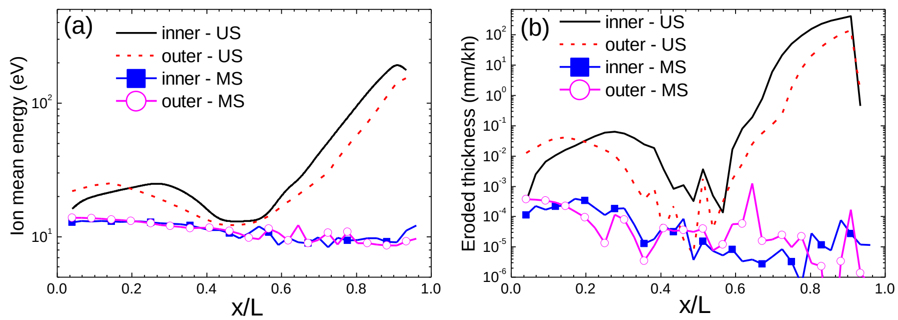

Figure 4. Axial profile of (a) ion kinetic energy impacting inner and outer walls, (b) eroded thickness estimation for 1000 hours of thruster operation for a threshold of sputtering of 30 eV, and for the US and MS configurations. The xenon mass flow is 1 mg.s^{-1} and the voltage 300 V.

IV. Conclusions and perspectives

We have modeled the operation of the ISCT-200 low-power Hall thruster whose channel geometry is chamfered at the end. Two magnetic field configurations have been tested. The first one corresponds to a standard topology with a zone of maximum of magnetic field located around the exhaust region of the channel (US - unshielded configuration). The second configuration has one with a zone of maximum of magnetic field displaced in the near field plume and the magnetic field lines are almost parallel to the walls connecting the anode region to the outer/inner exterior poles (MS - magnetic shielding configuration). The anomalous electron mobility profile has been fitted with the experimental measurements of the axial ion velocity at the channel centerline. The calculations have been performed for fixed discharge voltage (300 V) and mass flow (1 mg/s), for a discharge power of about 250 W.

Calculation results have permitted to revisit the general trends reported in the literature confirming a quasi-negligible erosion of channel walls. Also, but not detailed in that paper, a large production of doubly charged ions is noticed in the MS configuration, while very similar oscillation regimes of the discharge currents are observed. From the deeper analysis of time-averaged plasma properties, we have seen that the MS configuration leads to a simultaneous push of the ionization region towards the exhaust of the thruster and the acceleration region towards the near field plume. Inside the channel, the low potential drop induces a low electron temperature and magnetic field lines to be almost equipotential (compared to the unshielded configuration). In the US configuration, the ionization extends all over the radial direction, while, in the MS case, the ionization region is concentrated in the center of the channel. In the US case, the high Te is responsible for a large radial electric field and a large sheath potential drop inducing a high erosion rate. On the other hand, in the MS configuration, the specific positions of ionization source term and electric potential profiles lead to a high ion current impacting on walls. The advantage of the MS configuration is the relatively low radial electric field and electron temperature when they bombard the walls maintaining a low kinetic energy of ions close to or under the erosion threshold.

It could be advantageous to use the LIF diagnostic in two-dimensions to map both axial and radial components of ion velocity in the near field plume and to determine if the shifted ionization and acceleration regions is responsible for a larger beam divergence in MS configuration. Measurements of electron temperature are necessary to validate the very high calculated electron temperature in the MS configuration. The incoherent Thomson scattering diagnostic previously used in the context of fusion plasmas has been recently successfully used to measure electron properties on a cathode plasma source with a high sensitivity [19]. Such non-intrusive diagnostic is now planned to be used in HT discharges. The deviation of a constant electron temperature along magnetic field lines could also be checked. Calculations for different mass flow rates and discharge voltages will be performed. We finally intend to modify the magnetic field configuration in the shielded version of the ISCT-200 and its consequence on plasma and performance properties.

Acknowledgments

This work has been performed with the support of CNES, through the Research and Technology Program. L. Grimaud has benefited from a CNES and Région Centre PhD grant.

References

[1] R. W. Conversano, D. M. Goebel, R. R. Hofer, I. G. Mikellides, and R. E. Wirz, "Performance Analysis of a Low-Power Magnetically Shielded Hall Thruster: Experiments", Journal of Propulsion and Power **33**, 975 (2017).

[2] V. P. Kim, "Design Features and Operating Procedures in Advanced Morozov's Stationary Plasma Thrusters", Technical Physics **60**, 362 (2015).

[3] I. G. Mikellides, I. Katz, R. R. Hofer, D. M. Goebel, K. de Grys, and A. Mathers, "Magnetic shielding of the channel walls in a Hall plasma accelerator", Physics of Plasmas **18**, 033501 (2011).

[4] R. R. Hofer, D. M. Goebel, I. G. Mikellides, and I. Katz, "Magnetic shielding of a laboratory Hall thruster. I. Theory and validation", Journal of Applied Physics **115**, 043303 (2014).

[5] R. R. Hofer, D. M. Goebel, I. G. Mikellides, and I. Katz, Magnetic shielding of a laboratory Hall thruster. II. Experiments" Journal of Applied Physics **115**, 043304 (2014).

[6] L. Grimaud and S. Mazouffre, "Ion behavior in low-power magnetically shielded and unshielded Hall thrusters", Plasma Sources Science and Technology **26**, 055020 (2017).

[7] L. Grimaud and S. Mazouffre, "Conducting wall Hall thrusters in magnetic shielding and standard configurations"**,** Journal of Applied Physics **122**, 033305 (2017).

[8] S. Mazouffre and L. Grimaud, "Characteristics and Performances of a 100-W Hall Thruster for Microspacecraft", IEEE Transactions on Plasma Science **46**, 330 (2018).

[9] L. Garrigues, "Ion properties in a Hall current thruster operating at high voltage", Journal of Applied Physics **119**, 163305 (2016).

[10] L. Garrigues, G. Fubiani, and J. P. Boeuf, "Appropriate use of the particle-in-cell method in low temperature plasmas: Application to the simulation of negative ion extraction", Journal of Applied Physics **120**, 213303 (2016).

[11] M. Lampe, G. Joyce, W. M. Manheimer, and S. P. Slinker, "Quasi-neutral particle simulation of magnetized plasma discharges: general formalism and application to ECR discharges", IEEE Transactions on Plasma Science **26**, 1592 (1998).

[12] E. Ahedo, R. Santos, and F. I. Parra, "Fulfillment of the kinetic Bohm criterion in a quasineutral particle-in-cell model", Physics of Plasmas **17**, 073507 (2010).

[13] A. I. Morozov, Y. Esipchuk, G. Tilinin, A. Trofimov, Y. Sharov, and G. Y. Shchepkin, "Plasma Accelerator with Closed Electron Drift and Extended Acceleration Zone Soviet Physics Technical Physics **17**, 38 (1972).

[14] L. Garrigues, G. J. M. Hagelaar, C. Boniface, and J. P. Boeuf, "Anomalous conductivity and secondary electron emission in Hall effect thrusters" Journal of Applied Physics **100**, 123301 (2006).

[15] L. Garrigues, G. J. M. Hagelaar, J. Bareilles, C. Boniface, and J. P. Boeuf, "Model study of the influence of the magnetic field configuration on the performance and lifetime of a Hall thruster", Physics of Plasmas **10**, 4886 (2003).

[16] L. Garrigues, S. Mazouffre, and G. Bourgeois, "Computed versus measured ion velocity distribution functions in a Hall effect thruster", Journal of Applied Physics **111**, 113301 (2012).

[17] R. W. Conversano, D. M. Goebel, I. G. Mikellides, R. R. Hofer, and R. E. Wirz,, "Performance Analysis of a Low-Power Magnetically Shielded Hall Thruster: Computational Modeling", Journal of Propulsion and Power **33**, 992 (2017).

[18] L. Grimaud, S. Mazouffre, and C. Boniface, "Performance Comparison Between Standard and Magnetically Shielded 200 W Hall Thrusters with BN-SiO_2 and Graphite Channel Walls," *35^th^ International Electric Propulsion Conference*, Atlanta, GE, 2017, paper IEPC-2017-172.

[19] B. Vincent, S. Tsikata, S. Mazouffre, T. Minea, and J. Fils, "A compact new incoherent Thomson scattering diagnostic for low-temperature plasma studies", Plasma Sources Science and Technology **27**, 055002 (2018).